Supplementary information for

Diffusion–reaction competition governs zinc electrodeposition in three-dimensional carbon scaffolds

Qingyang Yin[1], Faith Ann Brookshire[1], Prof. Zheng Chen[1,2*]

[1] *Aiiso Yufeng Li Family Department of Chemical and Nano Engineering, University of California, San Diego, La Jolla, CA 92093, USA*

[2] *Sustainable Power and Energy Center, University of California, San Diego, La Jolla, CA 92093, USA*

[*] Corresponding author: zhc199@ucsd.edu

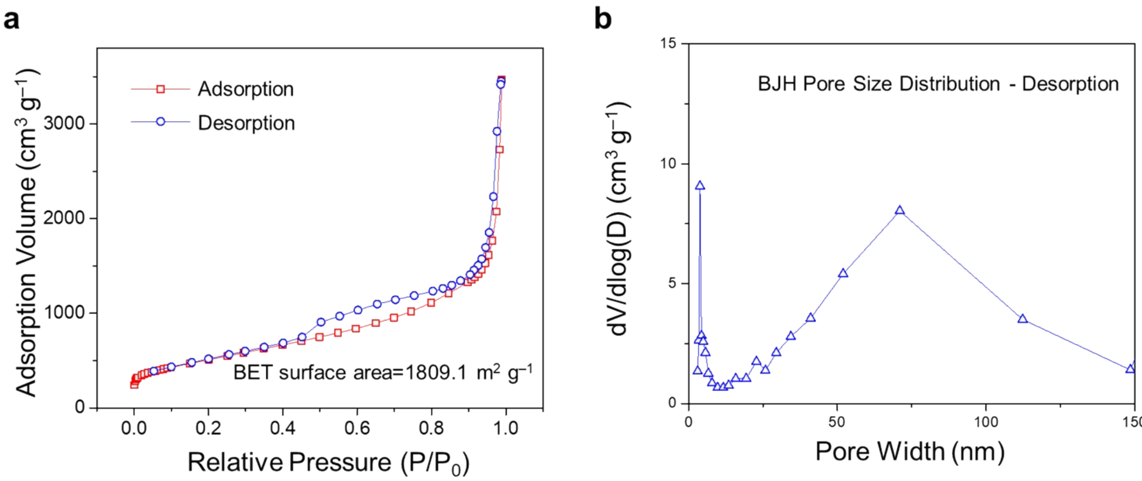

Fig. S1. (a) The BET surface area measured from N_2 adsorption-desorption isotherms of Ketjen Black (KB) and (b) the corresponding BJH pore size distribution.

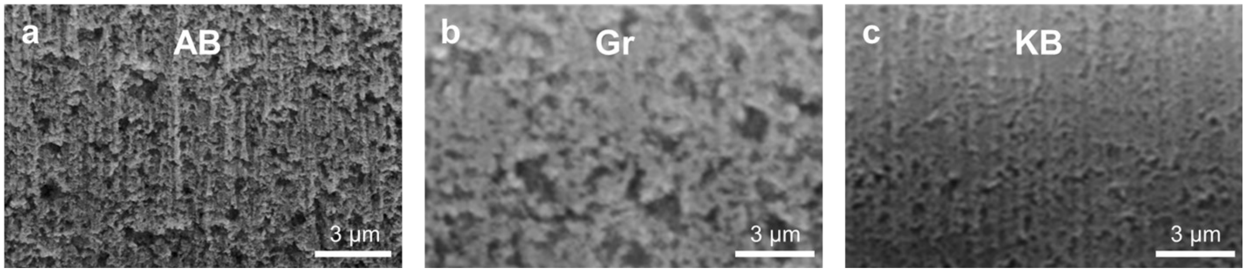

Fig. S2. Focused-ion beam scanning electron microscope (FIB–SEM) images of (a) acetylene black (AB), (b) graphene (Gr), and (c) KB-based scaffolds.

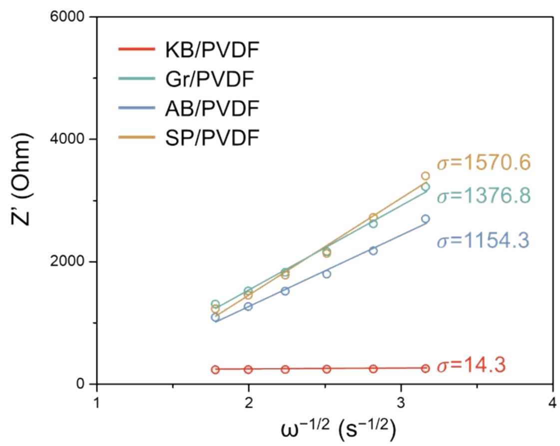

Fig. S3. Warburg coefficient (σ) extracted from the low-frequency region of the Nyquist plots.

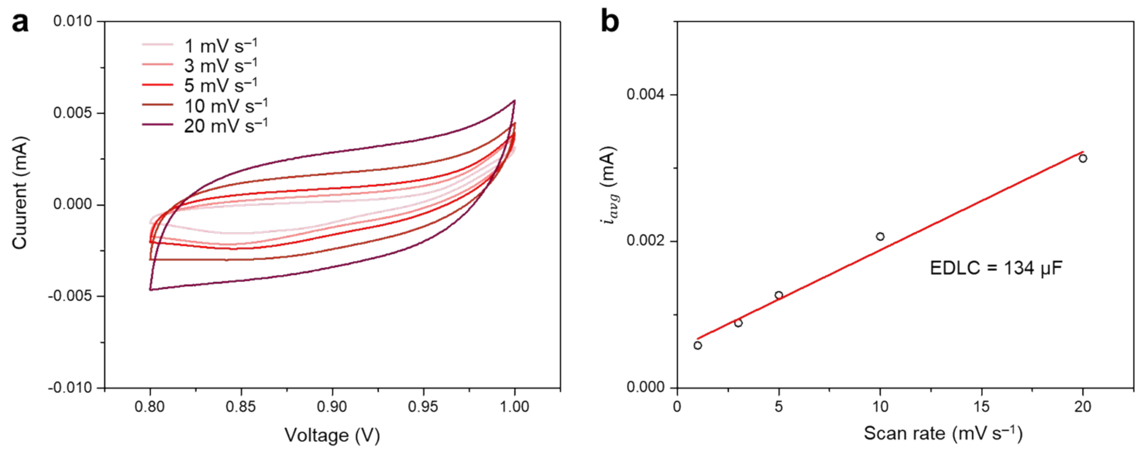

Fig. S4. (a) Cyclic voltammetry (CV) of Zn||acetylene black (AB)/PVDF at various scan rate. (b) Electrochemical double-layer capacitance (EDLC) determination of the AB/PVDF scaffold derived from the CV curves.

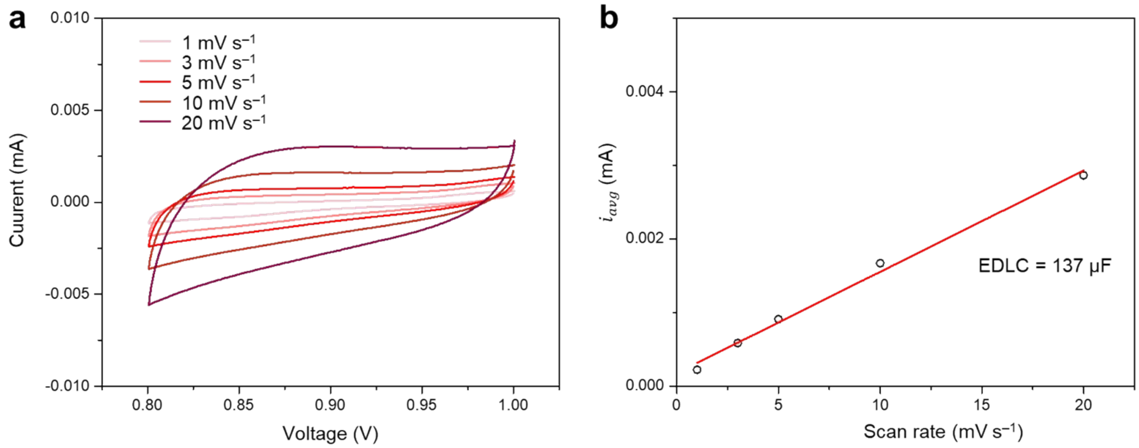

Fig. S5. (a) CV curves of Zn||Super P (SP)/PVDF at various scan rate. (b) EDLC determination of the SP/PVDF scaffold derived from the CV curves.

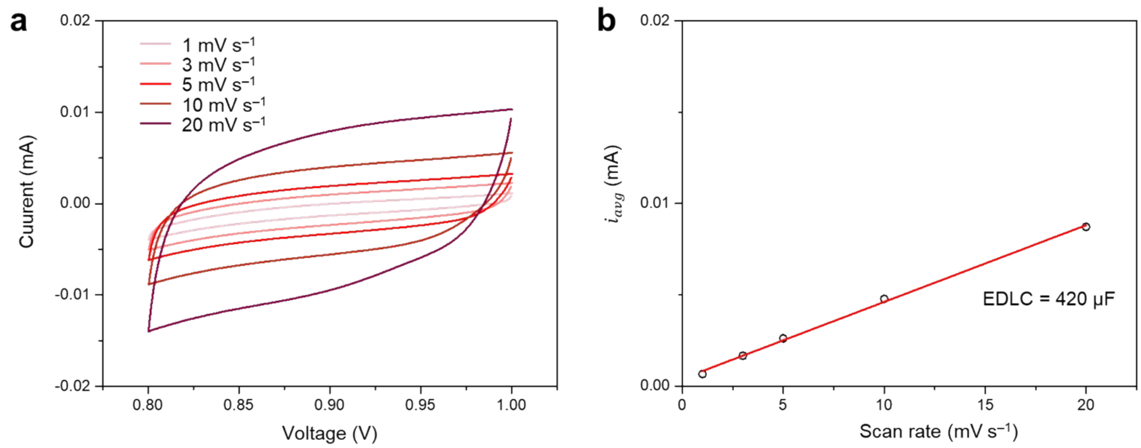

Fig. S6. (a) CV curves of Zn||graphene (Gr)/PVDF at various scan rate. (b) EDLC determination of the Gr/PVDF scaffold derived from the CV curves.

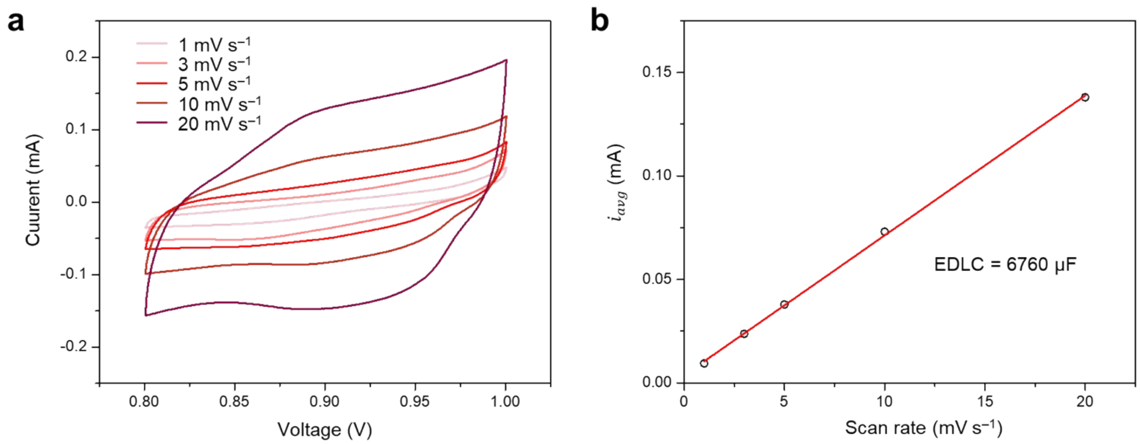

Fig. S7. (a) CV curves of Zn||Ketjen Black(KB)/PVDF at various scan rate. (b) EDLC determination of the KB/PVDF scaffold derived from the CV curves.

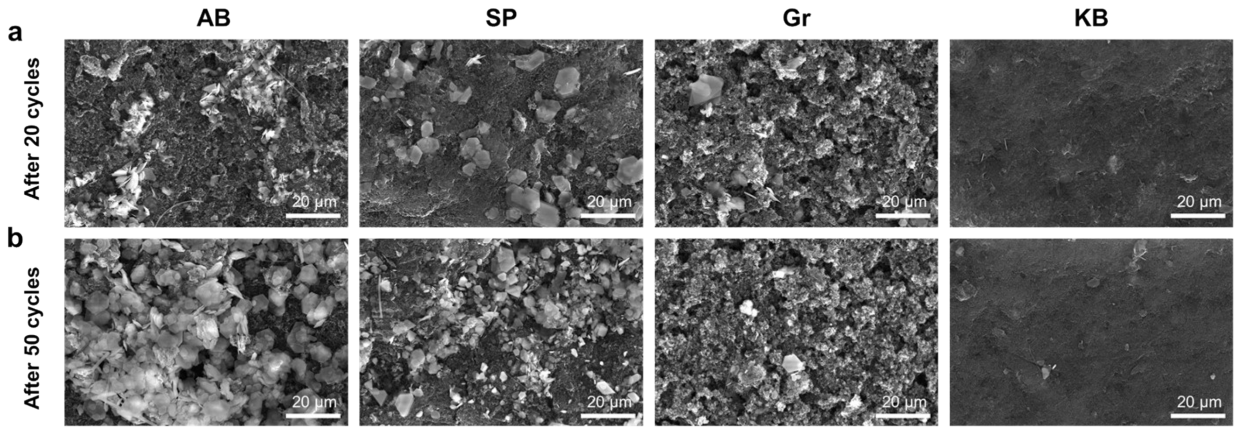

Fig. S8. SEM images of AB/PVDF, SP/PVDF, Gr/PVDF, and KB/PVDF (from left to right) after (a) 20 cycles and (b) 50 cycles of cycling at 2 mA cm^{-2}, 2 mAh cm^{-2}.

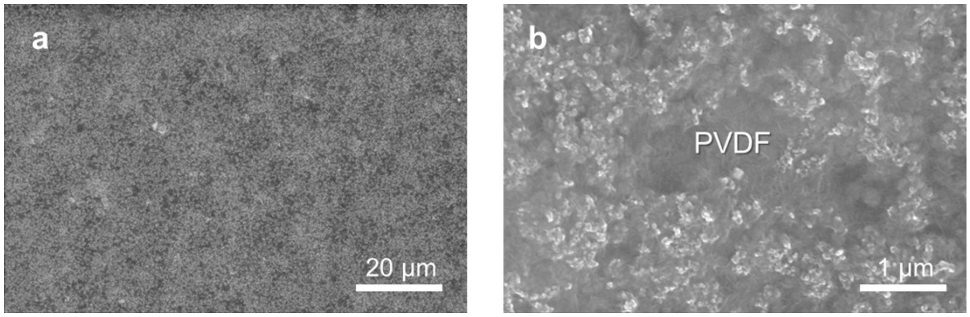

Fig. S9. SEM images of pristine KB5/PVDF5.

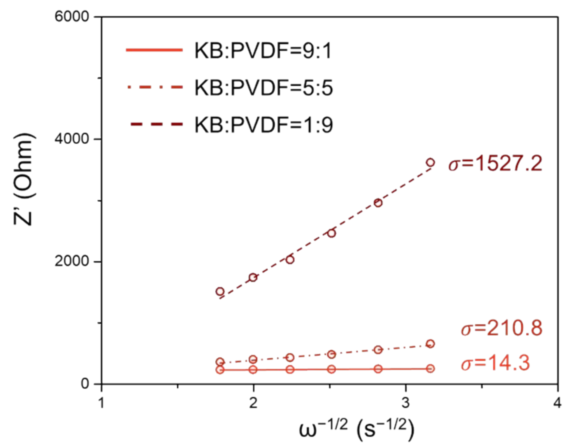

Fig. S10. σ of KB-based scaffolds with varying polymer fractions, extracted from the low-frequency region of the Nyquist plots.

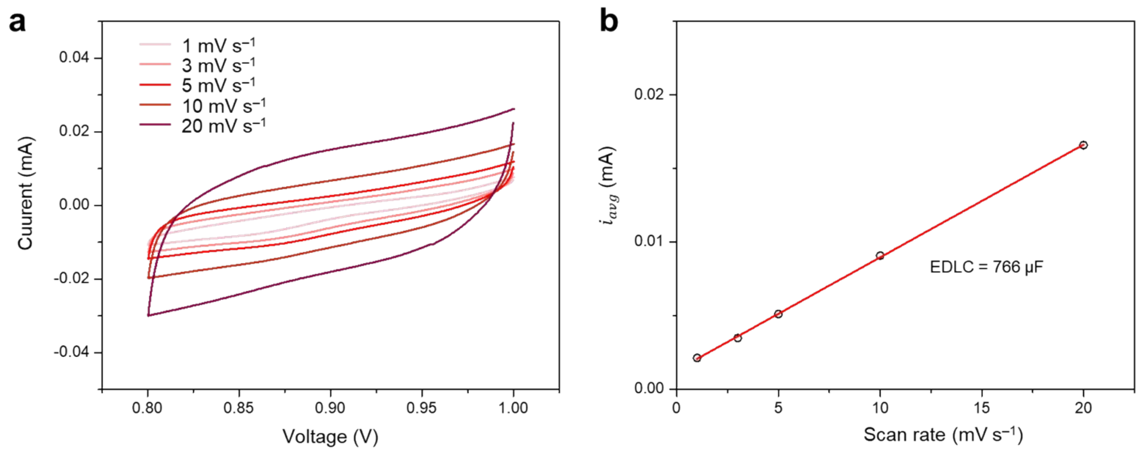

Fig. S11. (a) CV curves of Zn||KB5/PVDF5 at various scan rate. (b) EDLC determination of the KB5/PVDF5 scaffold derived from the CV curves.

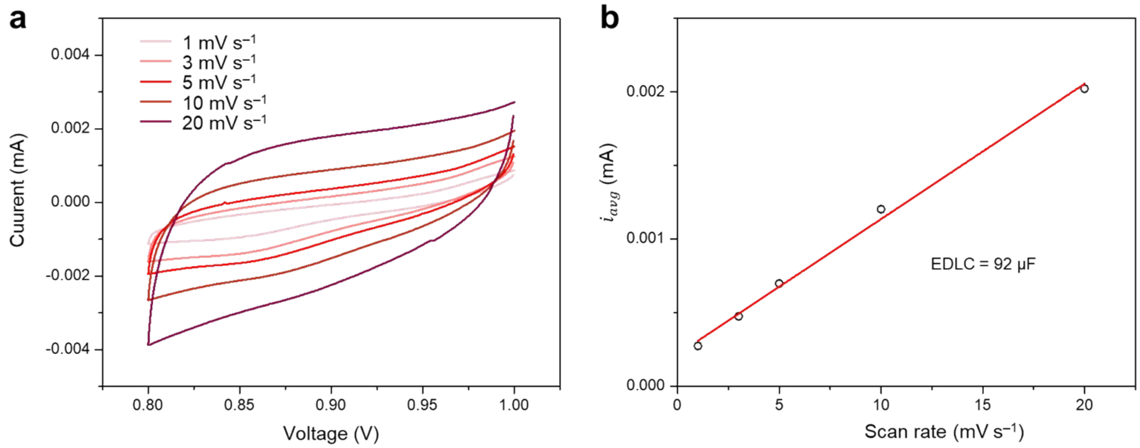

Fig. S12. (a) CV curves of Zn||KB1/PVDF9 at various scan rate. (b) EDLC determination of the KB1/PVDF9 scaffold derived from the CV curves.

Table S1. Warburg coefficient and apparent diffusion coefficient of scaffolds employing various carbon materials.

	Charge-transfer resistance (Ω)	Warburg coefficient, σ (Ω $s^{1/2}$)	Apparent diffusion coefficient (cm^2 s^{-1})
AB/PVDF	848.3	1154.3	6.7×10^{-16}
SP/PVDF	700.5	1570.6	3.6×10^{-16}
Gr/PVDF	694.9	1376.8	4.7×10^{-16}
KB/PVDF	222.2	14.3	4.4×10^{-12}

The σ was obtained by fitting the Z' vs. $\omega^{-1/2}$ profile in the low-frequency region of the Nyquist plot. The apparent diffusion coefficient (D_{app}) was calculated using equation:

$$D_{app} = \frac{R^2T^2}{2A^2n^4F^4C^2\sigma^2}$$

where R is the gas constant, T the absolute temperature, A the electrode area, n the valence number, F the Faraday constant, and C the bulk electrolyte concentration. Although this analysis relies on simplified assumptions, such as treating the low-frequency response as a semi-infinite diffusion regime and assuming uniform ion transport across the electrode, which cannot fully capture the complexities of porous electrodes, all four carbon-based scaffolds share comparable architectures and were tested under identical conditions. Therefore, the extracted values represent meaningful apparent diffusion coefficients for relative comparison.

Table S2. Warburg coefficient and apparent diffusion coefficient of KB-based scaffolds with varying polymer fractions.

	Charge-transfer resistance, R_{ct} (Ω)	Warburg coefficient, σ (Ω $s^{1/2}$)	Apparent diffusion coefficient (cm^2 s^{-1})
KB/PVDF	222.2	14.3	4.4×10^{-12}
KB5/PVDF5	334.3	210.8	2.0×10^{-14}
KB1/PVDF9	1043.1	1527.2	3.8×10^{-16}

Table S3. Diffusion coefficients and exchange current densities used for COMSOL simulations for each scaffold.

Scaffold	Diffusion coefficients ($cm^2\ s^{-1}$)	Exchange current densities ($A\ m^2$)
low σ and high ECSA	5×10^{-12}	5
Medium σ and ECSA	5×10^{-13}	10
High σ and low ECSA	5×10^{-14}	50

Table S4. Summary of state-of-the-art strategies employing 3D architectures to regulate Zn deposition.

Scaffold	Deposition mode	Current density & Areal capacity	CE performance	Ref.
KB@Cu	**Bottom-up**	**2 mA cm^{-2}, 2 mAh cm^{-2}**	**99.5%, 700 cycles**	**This work**
CNF-Zn	Uniform	2 mA cm^{-2}, 1 mAh cm^{-2}	99.5%, 450 cycles	[1]
Sn@NHCF	Uniform	5 mA cm^{-2}, 1 mAh cm^{-2}	99.5%, 600 cycles	[2]
Sn-PCF	Uniform	1 mA cm^{-2}, 1 mAh cm^{-2}	95%, 150 cycles	[3]
3D Cu@In	Uniform	0.5 mA cm^{-2}, 0.5 mAh cm^{-2}	98%, 300 cycles	[4]
3D graphene	Uniform	10 mA cm^{-2}, 1 mAh cm^{-2}	98.3%, 400 cycles	[5]
R-Cu_2O/CM	Uniform	2 mA cm^{-2}, 1 mAh cm^{-2}	99.25%, 400 cycles	[6]

Reference

1 J.-H. Wang, L.-F. Chen, W.-X. Dong, K. Zhang, Y.-F. Qu, J.-W. Qian and S.-H. Yu, *ACS Nano*, 2023, **17**, 19087–19097.

2 H. Yu, Y. Zeng, N. W. Li, D. Luan, L. Yu and X. W. (David) Lou, *Sci. Adv.*, **8**, eabm5766.

3 J.-L. Yang, P. Yang, W. Yan, J.-W. Zhao and H. J. Fan, *Energy Storage Mater.*, 2022, **51**, 259–265.

4 X.-Y. Fan, H. Yang, B. Feng, Y. Zhu, Y. Wu, R. Sun, L. Gou, J. Xie, D.-L. Li and Y.-L. Ding, *Chem. Eng. J.*, 2022, **445**, 136799.

5 B. Wu, B. Guo, Y. Chen, Y. Mu, H. Qu, M. Lin, J. Bai, T. Zhao and L. Zeng, *Energy Storage Mater.*, 2023, **54**, 75–84.

6 D. Liu, Q. Wang, W. Fang, G. Tian, X. Chen, H. Yue and S. Feng, *J. Mater. Chem. A*, 2025, **13**, 15118–15127.